ACS APPLIED MATERIALS & INTERFACES

Research Article

www.acsami.org

Synthesis and Microwave Absorption Properties of Yolk–Shell Microspheres with Magnetic Iron Oxide Cores and Hierarchical Copper Silicate Shells

Jiwei Liu, Jin Cheng, Renchao Che,* Junjie Xu, Mengmei Liu, and Zhengwang Liu

Department of Material Science and Laboratory of Advanced Materials, Fudan University, Shanghai 200438, China

Supporting Information

ABSTRACT: Yolk–shell microspheres with magnetic Fe_3O_4 cores and hierarchical copper silicate shells have been successfully synthesized by combining the versatile sol–gel process and hydrothermal reaction. Various yolk–shell microspheres with different core size and shell thickness can be readily synthesized by varying the experimental conditions. Compared to pure Fe_3O_4, the as-synthesized yolk–shell microspheres exhibit significantly enhanced microwave absorption properties in terms of both the maximum reflection loss value and the absorption bandwidth. The maximum reflection loss value of these yolk–shell microspheres can reach −23.5 dB at 7 GHz with a thickness of 2 mm, and the absorption bandwidths with reflection loss lower than −10 dB are up to 10.4 GHz. Owing to the large specific surface area, high porosity, and synergistic effect of both the magnetic Fe_3O_4 cores and hierarchical copper silicate shells, these unique yolk–shell microspheres may have the potential as high-efficient absorbers for microwave absorption applications.

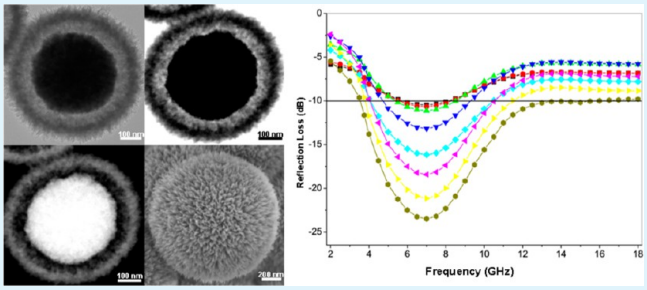

KEYWORDS: *yolk–shell, magnetite, copper silicate, hydrothermal synthesis, microwave absorption*

1. INTRODUCTION

Since the emergence of military products in the 1930s, electromagnetic interference (EMI) shielding materials have been widely used in military, industrial, and commercial fields.[1−7] To date, the demand for innovative EMI shielding has increased to meet growing needs for novel high-efficient microwave absorbers with lightweight, thin thickness, wide absorption bandwidth, and strong absorption characteristics.[8] As an important class of functional nanomaterials, magnetite (Fe_3O_4) nanoparticles have been extensively investigated as microwave absorbers with low cost and strong absorption characteristics.[9−12] However, the Fe_3O_4 materials have main disadvantages such as high density and narrow absorption bandwidth, which restrict their further applications. It has been reported that nanocomposites are appropriate for broadband lightweight absorbers.[13−15] Recently, many core–shell structured nanocomposites containing Fe_3O_4 cores (e.g., Fe_3O_4/C,[16] Fe_3O_4/ZnO,[17] Fe_3O_4/SnO_2,[18] or Fe_3O_4/TiO_2[19,20]) show the microwave absorption performance better than the pure core or shell materials. Very recently, Wang et al. have reported an atomic layer deposition strategy to coat carbon nanocoils with magnetic Fe_3O_4 or Ni for the synthesis of coaxial multilayer nanostructures, which exhibit remarkably improved microwave absorption properties compared to the pristine carbon nanocoils.[21] It is well-known that the absorption properties of a material are closely related to the structure of microwave absorber.[5,22] Recent advances show that excellent microwave absorption properties can be obtained from hierarchical nanostructures with complicated geometrical morphologies.[23,24] Nonetheless, it is still a big challenge to fabricate hierarchical nanostructures with desired composition, controllable core size, and well-defined shell structure, which can greatly enhance the microwave absorption performance.

Yolk–shell structures refer to hollow nanostructures with a void space between the core and the shell, which have recently attracted considerable attention in a wide range of applications including nanoreactors,[25−27] catalysis,[28,29] lithium-ion batteries,[30−32] and biomedical fields.[33−36] In considering their unique properties such as low density, large surface area, functional nanostructure, and synergistic effects of both the cores and shells, yolk–shell structures with magnetic Fe_3O_4 cores and hierarchical shells may have the potential to satisfy the increasing demand of lightweight, thin thickness, wide absorption bandwidth, and strong absorption characteristics for innovative EMI shielding systems.[8] More recently, we have reported a facile "hydrothermal-assisted crystallization" route to synthesize hierarchical magnetic yolk–shell microspheres with mixed barium silicate and barium titanium oxide shells, which are demonstrated to be attractive candidate materials for microwave absorption enhancement.[37] To the best of our

Received: December 10, 2012
Accepted: March 8, 2013
Published: March 8, 2013

knowledge, studies on the synthesis of Fe_3O_4-based yolk–shell structures for microwave absorption have been rarely reported. Importantly, an understanding of the relationship between the yolk–shell structure and the microwave absorption properties of these materials is therefore necessary in order to understand how to optimize the structure of microwave absorbers.

In this study, we report the synthesis of unique yolk–shell microspheres with magnetic Fe_3O_4 cores and hierarchical copper silicate shells (Fe_3O_4@CuSilicate). Various Fe_3O_4@CuSilicate yolk–shell microspheres with different core size and shell thickness can be successfully synthesized by varying the experimental conditions. When evaluated as microwave absorbers, the as-synthesized yolk–shell microspheres exhibit significantly enhanced microwave absorption properties in comparison with pure Fe_3O_4. Our results suggest that these unique yolk–shell microspheres with controllable size, composition, and structure can be effective in microwave absorption enhancement, which can also be extended to design other high-efficient absorbers for microwave absorption applications.

2. EXPERIMENTAL SECTION

2.1. Materials. Ferric chloride hexahydrate ($FeCl_3{\cdot}6H_2O$), copper nitrate ($Cu(NO_3)_2{\cdot}3H_2O$), ethylene glycol (EG), diethylene glycol (DEG), sodium acetate, trisodium citrate, tetraethyl orthosilicate (TEOS), ethanol, and ammonia solution (28 wt %) were all purchased from Shanghai Sinopharm Chemical Reagent Co., Ltd. All chemicals were of analytical grade and used without further purification. Deionized water obtained from Milli-Q system (Millipore, Bedford, MA) was used in all experiments.

2.2. Preparation of Uniform Fe_3O_4 Particles. The Fe_3O_4 particles were prepared by a solvothermal method as described previously.[20,37] Typically, $FeCl_3{\cdot}6H_2O$ (1.95 g, 7.2 mmol) and trisodium citrate (0.1 g) were first dissolved in EG (40 mL). A solution of 40 mL of DEG containing 4.0 g of sodium acetate was then added under stirring. After that, the mixture was stirred vigorously for 30 min and then transferred into a Teflon-lined stainless-steel autoclave with a capacity of 100 mL. The autoclave was heated at 200 °C and maintained for 10 h and then allowed to cool to room temperature. Finally, the black precipitates were washed with water and ethanol by magnetic decantation for four times and dried at 60 °C for 6 h in vacuum.

2.3. Synthesis of Fe_3O_4@SiO_2 Core–Shell Microspheres. The Fe_3O_4@SiO_2 microspheres were synthesized through a modified Stöber method.[37] Briefly, as-prepared Fe_3O_4 particles (0.1 g) were dispersed in a mixture of ethanol (40 mL), water (10 mL), and ammonia solution (1 mL). Afterward, 0.8 mL of TEOS was added dropwise, and the reaction was allowed to proceed for 10 h under stirring. The resulting Fe_3O_4@SiO_2 microspheres were washed with ethanol by magnetic decantation for four times and dried at 60 °C for 6 h in vacuum.

2.4. Synthesis of Fe_3O_4@CuSilicate Yolk–Shell Microspheres. The Fe_3O_4@Cusilicate yolk–shell microspheres were synthesized according to the previously reported method.[38] In a typical process, 0.02 g of the Fe_3O_4@SiO_2 microspheres were dispersed in 36 mL of water by ultrasonication for 20 min, followed by addition of 2 mL of ammonia solution under stirring. After stirring for 5 min, an aqueous $Cu(NO_3)_2$ solution (1.2 mL, 0.1 M) was added dropwise and stirred for another 5 min. Then, the mixed solution was transferred into a Teflon-lined stainless-steel autoclave with a capacity of 50 mL. The autoclave was heated at 120 °C for 12 h and then allowed to cool to room temperature. The products were centrifuged and rinsed with ethanol several times and dried at 60 °C for 12 h in vacuum. Finally, the powder was calcinated at 550 °C in Ar atmosphere for 2 h with a heating rate of 5 °C min^{-1} to obtain highly crystalline phase.

2.5. Characterization. The size and morphology of the products were characterized by a field-emission scanning electron microscope (FESEM, HITACHI, S-4800) and transmission electron microscope (TEM, JEOL, JEM-2100F). High-resolution TEM (HRTEM), selected-area electron diffraction (SAED), energy dispersive X-ray spectroscopy (EDS), bright-field and high angle annular dark-field scanning transmission electron microscopy (BF/HAADF-STEM) were performed on a JEOL JEM-2100F transmission electron microscope equipped with a postcolumn Gatan imaging filter (GIF-Tridium) at an acceleration voltage of 200 kV. Powder X-ray diffraction (XRD) measurements were acquired using a Bruker D8 X-ray diffractometer with Ni-filtered Cu Kα radiation (40 kV, 40 mA). Magnetic properties were determined with a superconducting quantum interference device (SQUID, Quantum Design) magnetometer. Nitrogen adsorption isotherm measurements were carried out at 77 K with a Micromeritics Tristar 3020 analyzer.

2.6. Electromagnetic Measurements. The composite samples used for electromagnetic measurements were prepared by mixing the products and epoxy resin (EP) in a mass ratio of 1:5. A portion of the composite was coated on an aluminum substrate (180 mm × 180 mm) with a thickness of 2 mm to measure the reflection loss of the samples. The remaining sample was molded into the hollow pipe of a rectangular waveguide cavity with dimensions of 10.2 mm × 2.9 mm × 1.2 mm for complex permittivity and permeability measurements at 8–18 GHz and molded into a coaxial waveguide with a size of 3 mm (inside) × 7 mm (outside) × 3 mm (height) for measurements at 2–8 GHz. The complex relative permittivity, permeability, and reflection loss were measured with an HP8510C vector network analyzer and a reflection loss measurement system in the 2–18 GHz range. According to the transmission line theory, the reflection loss (RL) values of different composites at a given frequency and thickness layer can be defined with the following equations:[16−18]

$$\mathrm{RL}(dB) = -20\log_{10}|(Z_{in} - 1)/(Z_{in} + 1)|$$

$$Z_{in} = \sqrt{\mu_r/\varepsilon_r}\,\tanh[-j(2\pi fd/c)\sqrt{\mu_r\varepsilon_r}]$$

where ε_r and μ_r are the relative complex permittivity and permeability of the absorber medium, f is the frequency of microwave in free space, c is the velocity of light, d is the coating thickness, and Z_{in} is the input impedance of the absorber.

3. RESULTS AND DISCUSSION

3.1. Synthesis and Characterization of Fe_3O_4@CuSilicate Yolk–Shell Microspheres. The strategy for synthesizing Fe_3O_4@CuSilicate yolk–shell microspheres is schematically depicted in Scheme 1. First, uniform Fe_3O_4 particles prepared via a solvothermal reaction were coated with silica layer by the Stöber method to obtain Fe_3O_4@SiO_2 core–shell microspheres. Second, the obtained Fe_3O_4@SiO_2 core–shell microspheres were hydrothermally treated in aqueous $Cu(NO_3)_2$ and ammonia solution at 120 °C, leading to the formation of Fe_3O_4@CuSilicate yolk–shell microspheres.

Scheme 1. Schematic Illustration of the Synthesis Procedure for the Fe_3O_4@CuSilicate Yolk–Shell Microspheres

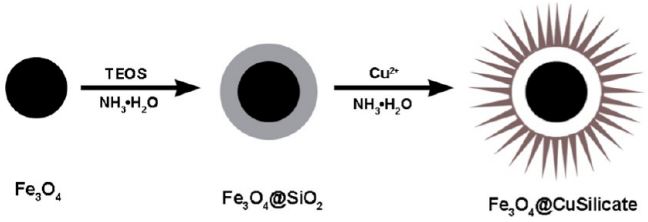

Figure 1a,b shows TEM and FESEM images of the Fe_3O_4 particles, which possess uniformly spherical shape and a mean

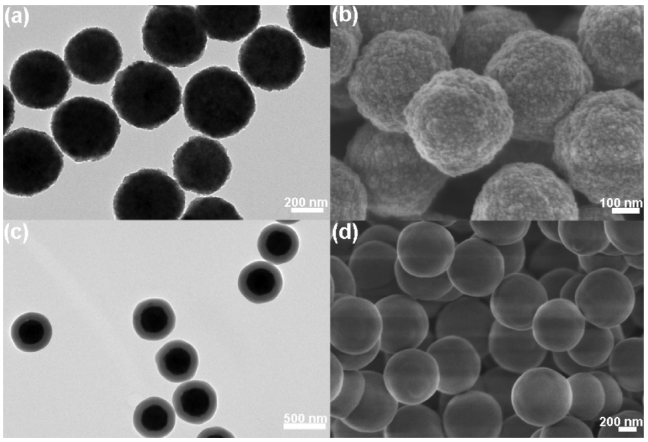

Figure 1. (a) TEM and (b) FESEM images of the Fe_3O_4 particles. (c) TEM and (d) FESEM images of the Fe_3O_4@SiO_2 core–shell microspheres.

diameter of ~450 nm. It can be clearly seen in the FESEM image that the Fe_3O_4 particles with very rough surface are actually composed of small primary nanocrystals. The volume ratio of EG/DEG (v/v in mL) controls the size of the Fe_3O_4 particles. For example, the ratios of 30/50 and 20/60 can lead to the synthesis of the Fe_3O_4 particles with average sizes of 330 and 150 nm, respectively (Figure S1, Supporting Information). By the use of the Stöber method, the Fe_3O_4 particles can be easily coated with a silica layer of ~120 nm in thickness (Figure 1c). Figure 1d shows the FESEM image of the obtained Fe_3O_4@SiO_2 core–shell microspheres. It can be seen that the Fe_3O_4@SiO_2 microspheres exhibit more regular spherical shape with smooth surface compared with the Fe_3O_4 particles, due to the deposition and growth of the silica layer. The thickness of the silica layer can be readily controlled by changing the TEOS amount. When the TEOS amount increases from 0.4 to 0.6 and 0.8 mL, the thickness of the silica layers for the Fe_3O_4@SiO_2 microspheres can be varied from ~92 to ~120 and ~145 nm, respectively (Figure S2, Supporting Information).

When hydrothermally treated in $Cu(NO_3)_2$ and ammonia solution, the SiO_2 layer of the Fe_3O_4@SiO_2 microspheres is gradually dissolved in the form of silicate anions. Driven by the interfacial reaction between Cu^{2+} cations and the silicate anions, CuSilicate nanograins are grown readily around the surface of the SiO_2 layer to form the CuSilicate shell. Herein, the SiO_2 layer serves not only as the precursor for the CuSilicate shell but also as a sacrificial template for the hollow structure.[39,40] After the hydrothermal reaction, the morphology of the Fe_3O_4@CuSilicate is examined by the FESEM. As shown in Figure 2a, the products exhibit an urchin-like shape with an average diameter of about 666 nm and consist of aligned needle-like nanosize primary particles. From a broken microsphere, unique yolk–shell structure with an interior core, an outer shell, and void space in between can be observed (Figure 2b). TEM further confirms that the synthesized microspheres possess a typical yolk–shell structure. It can be clearly seen in Figure 2c that the microspheres are composed of a dark particle individually encapsulated in ultrafine nanoneedle-assembled shells. The average size of the microspheres is approximately 670 nm, and the shell thickness is about 90 nm. EDS analysis of

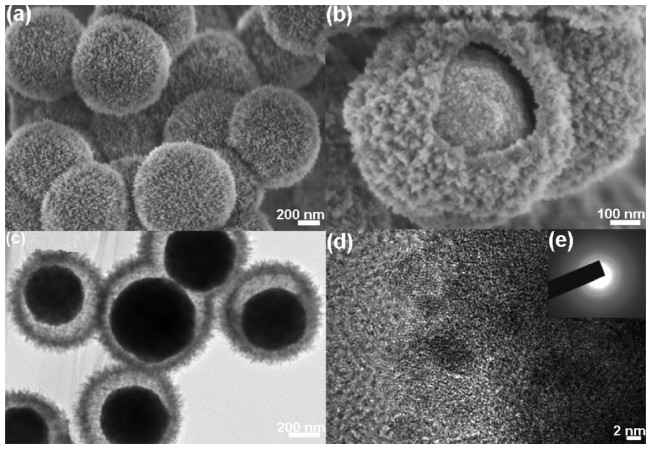

Figure 2. (a,b) FESEM and (c) TEM images of the Fe_3O_4@CuSilicate yolk–shell microspheres. (d) HRTEM image and (e) SAED pattern taken from the shell of the yolk–shell microspheres.

the yolk–shell microspheres indicates strong signals from Fe, O, Si, and Cu elements (Figure S3, Supporting Information). To further investigate their microstructure, BF/HAADF-STEM is employed. This unique yolk–shell structure is clearly demonstrated by the BF/HAADF-STEM images shown in Figure 3. Moreover, line scanning profiles reveal the actual

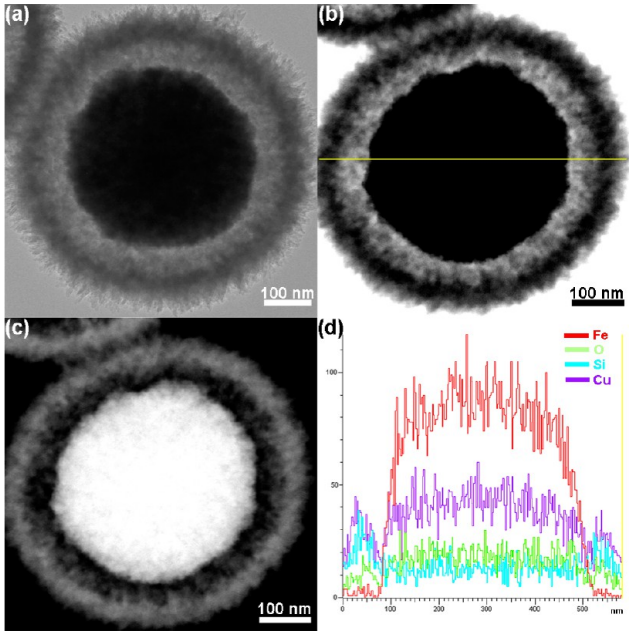

Figure 3. (a) TEM, (b) BF-STEM, and (c) HAADF-STEM images of an individual yolk–shell microsphere. (d) Line scanning profiles of Fe, O, Si, and Cu recorded along the line shown in (b).

distribution of Fe, O, Si, and Cu elements in the yolk–shell microsphere. The Fe element can be clearly seen in the core region, and the Cu and Si elements can be detected in the shell region, while the O element can be detected in both the core and shell regions.

The crystallographic structure and phase purity of the as-synthesized products are identified by XRD. Figure 4a shows the XRD pattern of the Fe_3O_4 particles. A few well-defined diffraction peaks at 2θ values of 18.3°, 30.1°, 35.4°, 37.1°, 43.1°, 53.4°, 56.9°, 62.5°, and 73.9° can be indexed to the (111),

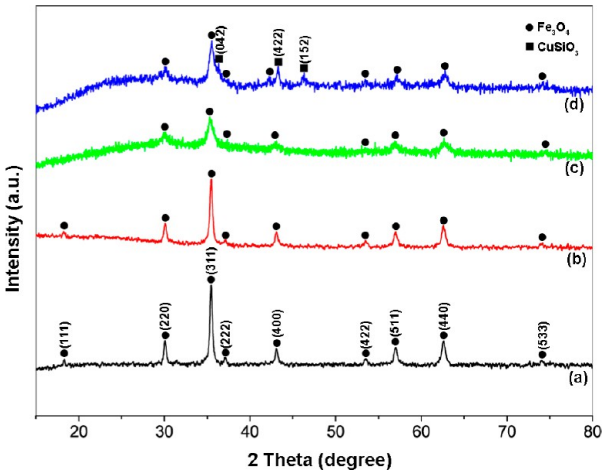

Figure 4. XRD patterns of the Fe_3O_4 particles (a), Fe_3O_4@SiO_2 microspheres (b), and Fe_3O_4@CuSilicate yolk–shell microspheres before (c) and after (d) annealing at 550 °C for 2 h.

(220), (311), (222), (400), (422), (511), (440), and (533) planes of cubic inverse spinel structure of magnetite (JCPDS card no. 19-0629). After coating with the SiO_2 layer, no characteristic peaks of other materials can be detected, indicating the SiO_2 layer is amorphous (Figure 4b). Figure 4c shows the XRD pattern of the as-synthesized yolk–shell microspheres. It can be found that there are no characteristic peaks of other materials, thereby suggesting that the hydrothermally synthesized nanoneedle-assembled shells are poorly crystalline. After annealing at 550 °C for 2 h, XRD pattern of the yolk–shell microspheres shows new characteristic diffraction peaks (Figure 4d). Three weak diffraction peaks at 2θ values of 36.9°, 44.9°, and 46.8° can be assigned to the (042), (422), and (152) planes of copper silicate (JCPDS card no. 32-0346). Moreover, the corresponding HRTEM image and SAED pattern recorded on the shell of the yolk–shell microspheres demonstrate that the shell is of high crystallinity, as shown in Figure 2d,e, respectively. It is worth mentioning that, even after the annealing at 550 °C, the yolk–shell microspheres still remain intact with almost no apparent collapse of the shell observed, indicating the excellent structural stability and integrity of the yolk–shell microspheres. On the basis of the SEM, TEM, BF/HAADF-STEM, and XRD results, it can be confirmed that the unique yolk–shell microspheres with spinel Fe_3O_4 cores and ultrafine nanoneedle-assembled copper silicate shells have been successfully synthesized.

In this work, the thicknesses of the copper silicate shells of these Fe_3O_4@CuSilicate yolk–shell microspheres can be readily tuned by the amount of $Cu(NO_3)_2$ and the SiO_2 layer thickness of the Fe_3O_4@SiO_2 templates used in the hydrothermal reaction. Figure 5a–d shows TEM images of the synthesized yolk–shell microspheres using the Fe_3O_4@SiO_2 microspheres with ~120 nm SiO_2 layer thickness as the templates. When the amount of $Cu(NO_3)_2$ increases from 0.6 to 0.9, 1.2, and 1.5 mL, the thickness of the copper silicate shells for the Fe_3O_4@CuSilicate yolk–shell microspheres (denoted as MCS-1, MCS-2, MCS-3, and MCS-4) can be varied from ~63 to ~75, ~90, and ~106 nm, respectively. Moreover, the copper silicate shells of the Fe_3O_4@CuSilicate yolk–shell microspheres are dependent on the SiO_2 layer thicknesses of the Fe_3O_4@SiO_2 templates. Under similar synthetic parameters to the synthesis of sample MCS-3, except for the use of the Fe_3O_4@SiO_2 microspheres with ~92 and ~145 nm SiO_2 layer thickness as the templates, the yolk–shell microspheres with ~55 and ~125 nm copper silicate shells can be synthesized. The corresponding products are denoted as MCS-5 and MCS-6, respectively, which are shown in Figure 5e,f.

Interestingly, the Fe_3O_4@CuSilicate yolk–shell microspheres with different core size and shell thickness can be synthesized using the Fe_3O_4@SiO_2 templates with different Fe_3O_4 core size and SiO_2 layer thickness. Figure 5g shows TEM image of the synthesized yolk–shell microspheres using the Fe_3O_4@SiO_2 microspheres with ~150 nm Fe_3O_4 core size and ~55 nm SiO_2 layer thickness as the templates (Figure S4a, Supporting Information). The average size of these yolk–shell microspheres (denoted as MCS-7) is about 250 nm, and the shell thickness is about 39 nm. As can be seen in Figure 5h, the yolk–shell microspheres with ~330 nm Fe_3O_4 core size and ~59 nm shell thickness (denoted as MCS-8) can also be produced when the Fe_3O_4@SiO_2 microspheres with ~330 nm Fe_3O_4 core size and ~118 nm SiO_2 layer thickness were used as the templates (Figure S4b, Supporting Information). Due to the high alterability of the Fe_3O_4 core size, SiO_2 coating thickness, and the amount of $Cu(NO_3)_2$, it is believed that the Fe_3O_4@CuSilicate yolk–shell microspheres with well-defined

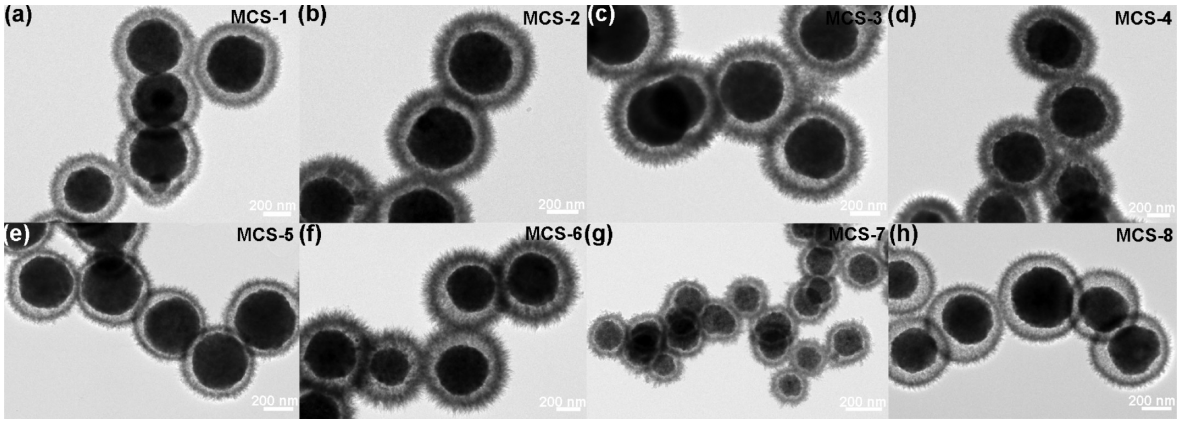

Figure 5. TEM images of the Fe_3O_4@CuSilicate yolk–shell microspheres with different Fe_3O_4 core sizes and copper silicate shell thicknesses: (a) ~450 nm core, ~63 nm shell, (b) ~450 nm core, ~75 nm shell, (c) ~450 nm core, ~90 nm shell, (d) ~450 nm core, ~106 nm shell, (e) ~450 nm core, ~55 nm shell, (f) ~450 nm core, ~125 nm shell, (g) ~150 nm core, ~39 nm shell, and (h) ~330 nm core, ~59 nm shell.

size and shell thickness can be rationally synthesized by this facile method.

The magnetic properties of the Fe_3O_4, Fe_3O_4@SiO_2, and Fe_3O_4@CuSilicate microspheres were investigated using a SQUID (Figure 6). Hysteresis loops of all the samples

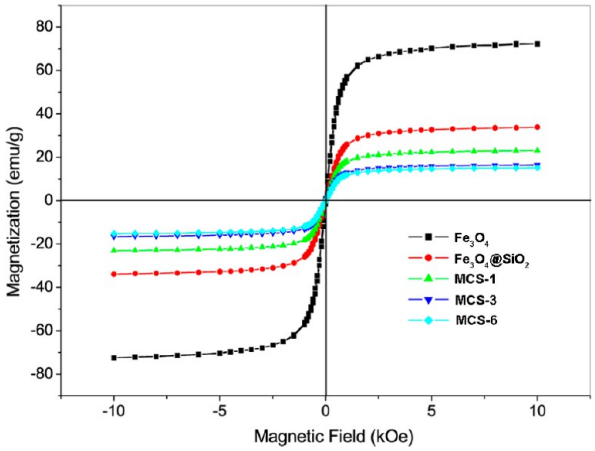

Figure 6. Hysteresis loops of the Fe_3O_4 particles, Fe_3O_4@SiO_2 microspheres, and Fe_3O_4@CuSilicate yolk–shell microspheres measured at 300 K.

measured at 300 K show no remanence or coercivity, suggesting a superparamagnetic character. The saturation magnetization (M_s) value of the Fe_3O_4 particles is estimated to be 72.2 emu g^{-1}. After coating with the SiO_2 layer, the M_s of the Fe_3O_4@SiO_2 microspheres decreases to 33.8 emu g^{-1}. The M_ss of the Fe_3O_4@CuSilicate yolk–shell microspheres for MCS-1, MCS-3, and MCS-6 are estimated to be 23.0, 16.5, and 15.2 emu g^{-1}, respectively. The much lower M_s of the Fe_3O_4@CuSilicate microspheres compared to the Fe_3O_4 particles can be attributed to the presence of nonmagnetic copper silicate shells in the microspheres. The thinner the shells, the stronger is the M_s of the Fe_3O_4@CuSilicate microspheres. N_2 sorption measurements show that the Fe_3O_4@CuSilicate yolk–shell microspheres have a mesoporous structure (Figure 7), derived from the packing of the ultrafine nanoneedles in the shells. As calculated by the Brunauer–Emmett–Teller (BET) method, such a yolk–shell structure gives rise to BET surface area of 135 m^2 g^{-1} and a relatively high pore volume of 0.22 cm^3 g^{-1},

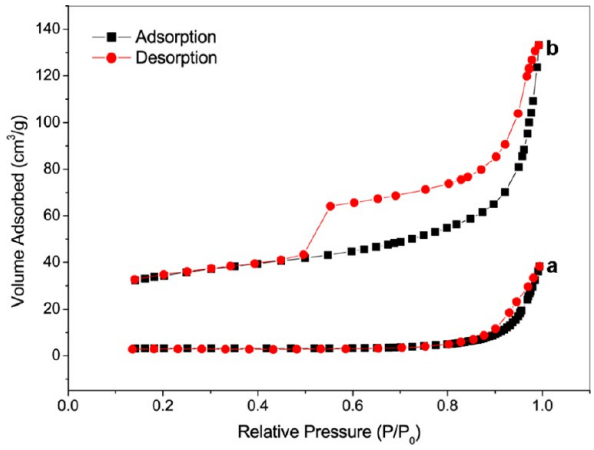

Figure 7. N_2 adsorption–desorption isotherms of the Fe_3O_4 particles (a) and Fe_3O_4@CuSilicate yolk–shell microspheres (b).

respectively, compared to 11 m^2 g^{-1} and 0.06 cm^3 g^{-1} for the Fe_3O_4 particles.

3.2. Microwave Absorption Properties of Fe_3O_4@CuSilicate Yolk–Shell Microspheres. To reveal the microwave absorption properties of the as-synthesized samples, the complex permittivity real part (ε'), permittivity imaginary part (ε''), permeability real part (μ'), and permeability imaginary part (μ'') of the EP composites containing the Fe_3O_4 particles and Fe_3O_4@CuSilicate yolk–shell microspheres were investigated in the frequency range of 2–18 GHz, as shown in Figure 8. Figure 9 shows the RL data for the Fe_3O_4/EP and Fe_3O_4@CuSilicate/EP composites. The values of maximum RL of the 150, 330, and 450 nm Fe_3O_4 particles are −10.2, −10.7, and −11.1 dB at 7 GHz with a thickness of 2 mm, respectively, while the Fe_3O_4@CuSilicate yolk–shell microspheres with 150, 330, and 450 nm Fe_3O_4 cores and 39, 59, and 63 nm copper silicate shells show maximum RL values of −13.2, −16.2, and −18.4 dB at 7 GHz with the same thickness, respectively. As can be seen, the Fe_3O_4@CuSilicate/EP composites display enhanced microwave absorption properties in terms of both the maximum RL values and the absorption bandwidths compared with the Fe_3O_4/EP composites. For example, the maximum RL value of the Fe_3O_4@CuSilicate yolk–shell microspheres with 450 nm Fe_3O_4 cores and 63 nm copper silicate shells is superior to that of the 450 nm Fe_3O_4 particles, with enhancement by about 66%. Moreover, the absorption bandwidths with RL lower than −10 dB increase from 3.2 to 6.6 GHz. Note that the maximum RL values of the Fe_3O_4@CuSilicate yolk–shell microspheres with 450 nm Fe_3O_4 cores and 90 and 125 nm copper silicate shells are −21.2 and −23.5 dB at 7 GHz with a thickness of 2 mm, respectively, and the absorption bandwidths with RL lower than −10 dB are up to 10.4 GHz (from 3.5 to 13.9 GHz). Compared with other reported Fe_3O_4-based materials,[16−19] the as-synthesized Fe_3O_4@CuSilicate yolk–shell microspheres manifest significantly enhanced microwave absorption properties with lower reflection loss and wider absorption bandwidths.

In our case, the enhanced microwave absorption properties may probably be attributed to the unique hierarchical yolk–shell structure. It is believed that the well-defined hierarchical nanostructures constructed by nanoneedle shells is believed to increase the geometrical absorption/scattering effect when a microwave is propagated inside these materials, thus leading to enhanced absorption abilities.[5,22] At the same time, the relatively large specific surface area and high porosity, as well as the void space existing in these yolk–shell microspheres can provide more active sites for reflection and scattering of microwave.[22,41,42] It can be seen in Figure 8a–d that the values of ε' for the Fe_3O_4@CuSilicate yolk–shell microspheres are less than those of the Fe_3O_4, while the values of ε'' are higher than those of the Fe_3O_4 in the whole frequency range. Moreover, we calculate the dielectric loss tangents ($\tan \delta_\varepsilon = \varepsilon''/\varepsilon'$) of the Fe_3O_4/EP and Fe_3O_4@CuSilicate/EP composites (Figure S5a, Supporting Information). The relatively high values of ε'' and $\tan \delta_\varepsilon$ imply that the Fe_3O_4@CuSilicate/EP composites exhibit intense dielectric losses, which might be attributed to such mechanisms as dominant dipolar polarization, interfacial polarization, and associated relaxation phenomena.[19,24] Generally, the excellent microwave absorptions are strongly dependent on the efficient complementarities between the relative permittivity and permeability.[18,43] Therefore, we calculate the magnetic loss tangents ($\tan \delta_\mu = \mu''/\mu'$) of the Fe_3O_4/EP and Fe_3O_4@CuSilicate/EP composites (Figure

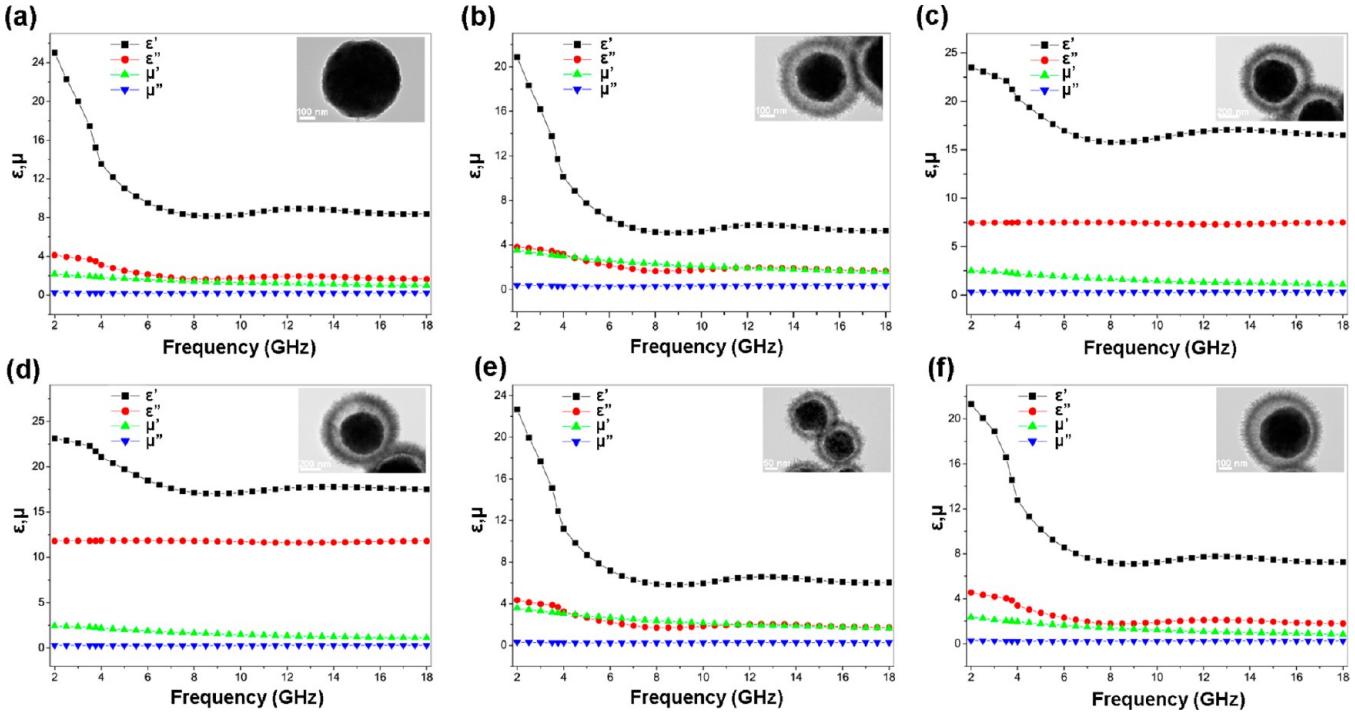

Figure 8. Frequency dependence of real and imaginary parts of complex permittivity and permeability of the EP composites containing the Fe_3O_4 particles and Fe_3O_4@CuSilicate yolk–shell microspheres: Fe_3O_4 (a), MCS-1 (b), MCS-3 (c), MCS-6 (d), MCS-7 (e), and MCS-8 (f).

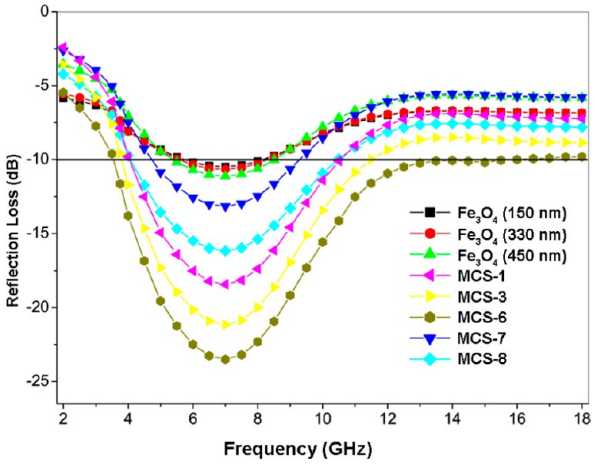

Figure 9. Microwave reflection loss curves of the EP composites containing the Fe_3O_4 particles and Fe_3O_4@CuSilicate yolk–shell microspheres.

S5b, Supporting Information). The significantly enhanced microwave absorption performance of the Fe_3O_4@CuSilicate yolk–shell microspheres with thicker shells may result from the nice dielectric behavior and effective complementarities between the dielectric loss and the magnetic loss, which originate from the synergistic effect of both the Fe_3O_4 cores and copper silicate shells.[20,23,37,43] All these results suggest that this hierarchical yolk–shell structure can effectively improve the microwave absorption properties of Fe_3O_4-based materials, which might be attractive candidate materials for microwave absorption applications.

4. CONCLUSIONS

In summary, we have demonstrated the synthesis of unique yolk–shell microspheres with magnetic Fe_3O_4 cores and hierarchical copper silicate shells by combining the versatile sol–gel process and hydrothermal reaction. Various yolk–shell microspheres with different core size and shell thickness have been successfully synthesized by varying the experimental conditions. Moreover, the as-synthesized yolk–shell microspheres exhibit significantly enhanced microwave absorption properties in comparison with pure Fe_3O_4 due to the large specific surface area, high porosity, and synergistic effect of both the magnetic Fe_3O_4 cores and hierarchical copper silicate shells. It is believed that the microwave absorption properties of these yolk–shell microspheres can be further optimized by tuning the size, composition, and morphology of both the interior core and outer shells, which may open up new opportunities for synthesizing novel high-efficient absorbers for microwave absorption applications.

■ ASSOCIATED CONTENT

Ⓢ Supporting Information

TEM images of the Fe_3O_4 particles with different sizes, TEM images of the Fe_3O_4@SiO_2 microspheres with different SiO_2 layer thicknesses, EDS pattern of the Fe_3O_4@CuSilicate yolk–shell microspheres, and frequency dependence of dielectric loss tangents and magnetic loss tangents of different samples. This information is available free of charge via the Internet at http://pubs.acs.org.

■ AUTHOR INFORMATION

Corresponding Author

*Tel: + 86 21 5163 0213. E-mail: rcche@fudan.edu.cn.

Notes

The authors declare no competing financial interest.

■ ACKNOWLEDGMENTS

This work was supported by the National Natural Foundation of China (Nos. 11274066, 51172047, 50872145, and

51102050), National Science Foundation for Postdoctoral Scientists of China (Grant No. 20110490647), and the Ministry of Science and Technology of China (973 Project Nos. 2013CB932901 and 2009CB930803). The authors are grateful to the "Shu Guang" project supported by Shanghai Municipal Education Commission and Shanghai Education Development Foundation (09SG01).

REFERENCES

(1) Pardavi, H. M. *J. Magn. Magn. Mater.* **2000**, *215*, 171.
(2) Ghasemi, A.; Morisako, A. *J. Magn. Magn. Mater.* **2008**, *320*, 1167.
(3) Wang, C.; Han, X. J.; Xu, P.; Wang, J. Y.; Du, Y. C.; Wang, X. H.; Qin, W.; Zhang, T. *J. Phys. Chem. C* **2010**, *114*, 3196.
(4) Wang, Z. H.; Han, Z.; Geng, D. Y.; Zhang, Z. D. *Chem. Phys. Lett.* **2010**, *489*, 187.
(5) Li, H. F.; Huang, Y. H.; Sun, G. B.; Yan, X. Q.; Yang, Y.; Wang, J.; Zhang, Y. *J. Phys. Chem. C* **2010**, *114*, 10088.
(6) Yan, S. J.; Zhen, L.; Xu, C. Y.; Jiang, J. T.; Shao, W. Z.; Tang, J. K. *J. Magn. Magn. Mater.* **2011**, *323*, 515.
(7) Zhu, Y. F.; Zhang, L.; Natsuki, T.; Fu, Y. Q.; Ni, Q. Q. *Synth. Met.* **2012**, *162*, 337.
(8) Huo, J.; Wang, L.; Yu, H. J. *J. Mater. Sci.* **2009**, *44*, 3917.
(9) Jia, K.; Zhao, R.; Zhong, J. C.; Liu, X. B. *J. Magn. Magn. Mater.* **2010**, *322*, 2167.
(10) Ni, S. B.; Sun, X. L.; Wang, X. H.; Zhou, G..; Yang, F.; Wang, J. M.; He, D. Y. *Mater. Chem. Phys.* **2010**, *124*, 353.
(11) Li, X. A.; Zhang, B.; Ju, C. H.; Han, X. J.; Du, Y. C.; Xu, P. *J. Phys. Chem. C* **2011**, *115*, 12350.
(12) Wang, F. L.; Liu, J. R.; Kong, J.; Zhang, Z. J.; Wang, X. Z.; Itoh, M.; Machida, K. *J. Mater. Chem.* **2011**, *21*, 4314.
(13) Ohlan, A.; Singh, K.; Chandra, A.; Dhawan, S. K. *ACS Appl. Mater. Interfaces* **2010**, *2*, 927.
(14) An, Z. G.; Pan, S. L.; Zhang, J. J. *J. Phys. Chem. C* **2009**, *113*, 2715.
(15) Cao, J.; Fu, W. Y.; Yang, H. B.; Yu, Q. J.; Zhang, Y. Y.; Liu, S. K.; Sun, P.; Zhou, X. M.; Leng, Y.; Wang, S. M.; Liu, B. B.; Zou, G. T. *J. Phys. Chem. B* **2009**, *113*, 4642.
(16) Chen, Y. J.; Xiao, G.; Wang, T. S.; Ouyang, Q. Y.; Qi, L. H.; Ma, Y.; Gao, P.; Zhu, C. L.; Cao, M. S.; Jin, H. B. *J. Phys. Chem. C* **2011**, *115*, 13603.
(17) Chen, Y. J.; Zhang, F.; Zhao, G. G.; Fang, X. Y.; Jin, H. B.; Gao, P.; Zhu, C. L.; Cao, M. S.; Xiao, G. *J. Phys. Chem. C* **2010**, *114*, 9239.
(18) Chen, Y. J.; Gao, P.; Wang, R. X.; Zhu, C. L.; Wang, L. J.; Cao, M. S.; Jin, H. B. *J. Phys. Chem. C* **2009**, *113*, 10061.
(19) Zhu, C. L.; Zhang, M. L.; Qiao, Y. J.; Xiao, G.; Zhang, F.; Chen, Y. J. *J. Phys. Chem. C* **2010**, *114*, 16229.
(20) Liu, J. W.; Che, R. C.; Chen, H. J.; Zhang, F.; Xia, F.; Wu, Q. S.; Wang, M. *Small* **2012**, *8*, 1214.
(21) Wang, G. Z.; Gao, Z.; Tang, S. W.; Chen, C. Q.; Duan, F. F.; Zhao, S. C.; Lin, S. W.; Feng, Y. H.; Zhou, L.; Qin, Y. *ACS Nano* **2012**, *6*, 11009.
(22) Qi, X. S.; Deng, Y.; Zhong, W.; Yang, Y.; Qin, C.; Au, C.; Du, Y. W. *J. Phys. Chem. C* **2010**, *114*, 808.
(23) Zhou, M.; Zhang, X.; Wei, J. M.; Zhao, S. L.; Wang, L.; Feng, B. X. *J. Phys. Chem. C* **2011**, *115*, 1398.
(24) Sun, G. B.; Dong, B. X.; Cao, M. H.; Wei, B. Q.; Hu, C. W. *Chem. Mater.* **2011**, *23*, 1587.
(25) Kamata, K.; Lu, Y.; Xia, Y. N. *J. Am. Chem. Soc.* **2003**, *125*, 2384.
(26) Liu, J.; Qiao, S. Z.; Hartono, S. B.; Lu, G. Q. *Angew. Chem., Int. Ed.* **2010**, *49*, 4981.
(27) Tan, L. F.; Chen, D.; Liu, H. Y.; Tang, F. Q. *Adv. Mater.* **2010**, *22*, 4885.
(28) Galeano, C.; Güttel, R.; Paul, M.; Arnal, P.; Lu, A. H.; Schüth, F. *Chem.—Eur. J.* **2011**, *17*, 8434.
(29) Lee, I.; Joo, J. B.; Yin, Y. D.; Zaera, F. *Angew. Chem., Int. Ed.* **2011**, *50*, 10208.
(30) Liu, J.; Xia, H.; Xue, D. F.; Lu, L. *J. Am. Chem. Soc.* **2009**, *131*, 12086.
(31) Liu, J.; Zhou, Y.; Wang, J.; Xue, D. *Chem. Commun.* **2011**, *47*, 10380.
(32) Liu, N.; Wu, H.; McDowell, M. T.; Yao, Y.; Wang, C. M.; Cui, Y. *Nano Lett.* **2012**, *12*, 3315.
(33) Zhao, W.; Chen, H.; Li, Y.; Li, L.; Lang, M.; Shi, J. *Adv. Funct. Mater* **2008**, *18*, 2780.
(34) Zhang, L. Y.; Wang, T. T.; Li, L.; Wang, C. G.; Su, Z. M.; Li, J. *Chem. Commun.* **2012**, *48*, 8706.
(35) Gao, J. H.; Liang, G. L.; Cheung, J. S.; Pan, Y.; Kuang, Y.; Zhao, F.; Zhang, B.; Zhang, X. X.; Wu, E. X.; Xu, B. *J. Am. Chem. Soc.* **2008**, *130*, 11828.
(36) Zhang, F.; Stucky, G.; Braun, G. B.; Shi, Y. F.; Zhang, Y. C.; Sun, X. H.; Reich, N. O.; Zhao, D. Y. *J. Am. Chem. Soc.* **2010**, *132*, 2850.
(37) Liu, J. W.; Xu, J. J.; Che, R. C.; Chen, H. J.; Liu, Z. W.; Xia, F. *J. Mater. Chem.* **2012**, *22*, 9277.
(38) Zhu, T.; Xia, B.; Zhou, L.; Lou, X. W. *J. Mater. Chem.* **2012**, *22*, 7851.
(39) Fang, Q. L.; Xuan, S. H.; Jiang, W. Q.; Gong, X. L. *Adv. Funct. Mater* **2011**, *21*, 1902.
(40) Zhu, T.; Wang, Z. Y.; Ding, S. J.; Chen, J. S.; Lou, X. W. *RSC Adv.* **2011**, *1*, 397.
(41) Guo, X. H.; Deng, Y. H.; Gu, D.; Che, R. C.; Zhao, D. Y. *J. Mater. Chem.* **2009**, *19*, 6706.
(42) Qin, Y.; Che, R. C.; Liang, C. Y.; Zhang, J.; Wen, Z. W. *J. Mater. Chem.* **2011**, *21*, 3960.
(43) Chen, Y. J.; Gao, P.; Zhu, C. L.; Wang, R. X.; Wang, L. J.; Cao, M. S.; Fang, X. Y. *J. Appl. Phys.* **2009**, *106*, 054303.